metals

MDPI

Article

A Study on the Stability Fields of Arc Plasma in the HPSR Process

Michael Andreas Zarl [1,*], Manuel Andreas Farkas [1] and Johannes Schenk [1,2]

[1] Department of Metallurgy, Chair of Ferrous Metallurgy, Montanuniversitaet Leoben, 8700 Leoben, Austria; Manuel-Andreas.Farkas@unileoben.ac.at (M.A.F.); Johannes.Schenk@unileoben.ac.at (J.S.)
[2] K1-MET GmbH, Stahlstraße 14, A-4020 Linz, Austria
* Correspondence: Michael-Andreas.Zarl@unileoben.ac.at

Received: 22 September 2020; Accepted: 12 October 2020; Published: 20 October 2020

Abstract: One of the major challenges for Europe's future steel production will be minimizing the inherent process emissions in the production of crude steel based on iron ores. In this case, mainly the reduction of CO_2 emissions is a focus. One promising process to overcome these problems is the hydrogen plasma smelting reduction (HPSR) process. This process has been studied for several years already at the Chair of Ferrous Metallurgy at Montanuniversitaet Leoben. The work presented focused on the stability of plasma arcs in the DC transferred arc system of the HPSR process. The stable operating plasma arc is of utmost importance for the future development of the process. The major objective is the definition of the most favorable conditions for this kind of arc. Therefore, tests were conducted to define fields of a stable operating plasma arc for multiple gas compositions and process variables. For several gas compositions of argon, nitrogen, argon/nitrogen, argon/hydrogen and nitrogen/hydrogen, fields of stability were measured and defined. Besides, the major influencing parameters and trends for the fields of stability were evaluated and are shown in this work.

Keywords: arc plasma; arc stability; smelting reduction; iron ore; hydrogen reduction

1. Introduction

Among the most important factors for the future of the European steel industry is decreasing the specific CO_2 emissions per ton of steel. CO_2 emissions have, with a share of 86% (in the year 2018: industry, fuels, forestry and other land use) of the total greenhouse gas emissions, serious consequences on Earth's flora and fauna. This 86% is equal to 43.7 Gt of CO_2 equivalent [1]. In 2018, the share of the global steel sector was estimated to be 3.5 Gt CO_2 [2]. This means that the steel sector was responsible for more than 8% of the world's anthropogenic CO_2 emissions in 2018. The production of liquid steel in Europe can only exist in the future with a significant reduction of at least 80% of the CO_2 emissions [3]. For the reduction of iron oxides, the common process route (blast furnace (BF), basic oxygen furnace (BOF)) is reaching its limits concerning the minimization of emissions. Modern integrated steelworks produce crude steel at the specific emission of 1.8 t of CO_2 per t of liquid crude steel at best practice [4]. The aforementioned reduction of 80% is, without further processing of the off-gas, not reachable (e.g., carbon capture and utilization (CCU)). To solve this problem, the smelting reduction of iron oxides using hydrogen plasma smelting reduction (HPSR) could be an alternative production route. HPSR is a one-step steel production process that uses the very high reduction potential of mainly excited but also ionized hydrogen to reduce iron ore with a minimum of CO_2 emissions [5]. The process has been studied at Montanuniversitaet Leoben in Austria since 1992 [6–9]. Previous works have already shown that the production of steel using a hydrogen plasma can not only reduce emissions significantly; it also has the potential to produce steel in a single-step process at ~ 15–20% lower costs than the common integrated route. The process

is currently underway and the state-of-the-art small bench-scale facility produces around 65–70 kg of steel out of 100 kg iron ore fines per hour. The predecessor facility in the Chair of Ferrous Metallurgy's lab operates at around 200 g of iron ore fines per hour. The objective of the current development is to develop a theory for the comparison and relation of the results and parameters between the two facilities. With this approach, the results of the lab facility should be transferable towards the bench-scale plant. This would both ease the conduction of bigger testing campaigns and decrease future development costs drastically. For the implementation of the linking parameters, scale-up factors and comparative cases should be evaluated and defined. Among the most important factors for the realization of the process on a bigger scale is the stability of the plasma arc. For the definition of a criterion for the stability of the DC transferred arc, the influencing parameters need to be investigated. The investigation focuses on the parameters' arc length, maximum current of the electric power supply, gas flow and composition as well as the feed of iron ore fines through the arc which determine the fields of stable plasma arc operation. Figure 1 shows a theoretical example of such a stability field which is defined by the parameters' voltage, current and arc length. The green-patterned area shows the field of the stable operation of the arc which is characterized by the fact that the voltage correlates almost linearly with the arc length. At lower arc lengths, the field is limited by the minimum power input required for the ionization of the gas in the arc (point A), whereas at the longest arc length, the limitation is the maximum voltage level after the transformer and rectifier of the power unit (point B). The maximum power input is mainly defined by the gas composition and the arc length, which determines point C. The maximum current at the lowest operable arc length sets point D. (Note: the operable arc length must not be zero). The operation of the facility in the stability field is possible by the adjustment of both the supplied current with the silicon-controlled rectifier (SCR) power controller and the arc length. It has to be emphasized that this stable field is only valid for the given gas composition and flow.

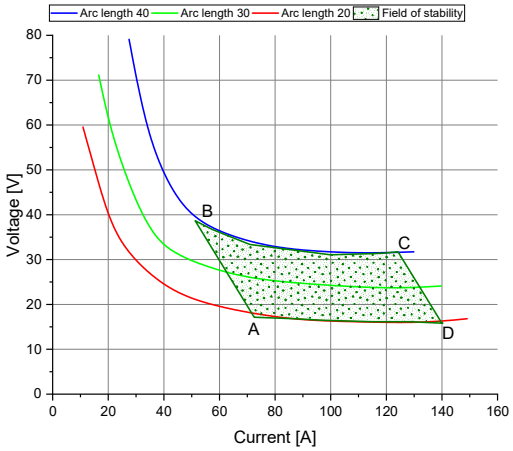

Figure 1. Example of a field of stability for the DC transferred arc.

2. Arc Plasma Basics for the HPSR Process

If the energy of a substance is permanently increased, it changes its state of matter from solid to liquid to gaseous and finally to the fourth state of matter, the so-called plasma state. In some exceptional cases, the state of matter can change from solid directly to gaseous. The first two transitions (solid–liquid, liquid–gas) are isothermal transitions where dT/dt at the melting temperature or the boiling point is constant zero. The transition to a plasma state is not an isothermal step. Therefore, it is a continuous transformation at rising temperatures. Due to this, it is impossible to define the state of plasma in association with a single temperature precisely. Only a certain degree of ionization of the particles can be associated with a single temperature. The most important parameters for the definition of plasmas are [10]:

- Free ions and electrons;

- Electrical conductivity;
- Magnetic force;
- Light and photon emission.

2.1. HPSR Basics of Thermodynamics and Kinetics

The thermodynamic principles and the basic operation of the HPSR process have been explained several times in multiple previous works [11–16]. Therefore, only the most important aspects are mentioned in the present work. The focus relies on thermodynamics because the temperature field of the arc is strongly connected to the thermodynamics of the process. Hydrogen shows many different forms in the transition to the plasma state. The forms and their potentials for reduction (left to right shows high to low, respectively) are as follows [16]:

$$H^+ > H_2^+ > H_3^+ > H > H_2 \quad (1)$$

Additionally, excited forms (e.g., H*) of each step in the ionization process can occur. These excited forms show either a rotational or a vibrational behavior. In some cases, they show both patterns. This state is called rovibrational [17]. The transition of molecular hydrogen towards the atomic state already starts at temperatures below 2000 °C. Figure 2 shows the thermodynamic equilibrium of 0.5 moles of hydrogen and argon against temperature [14].

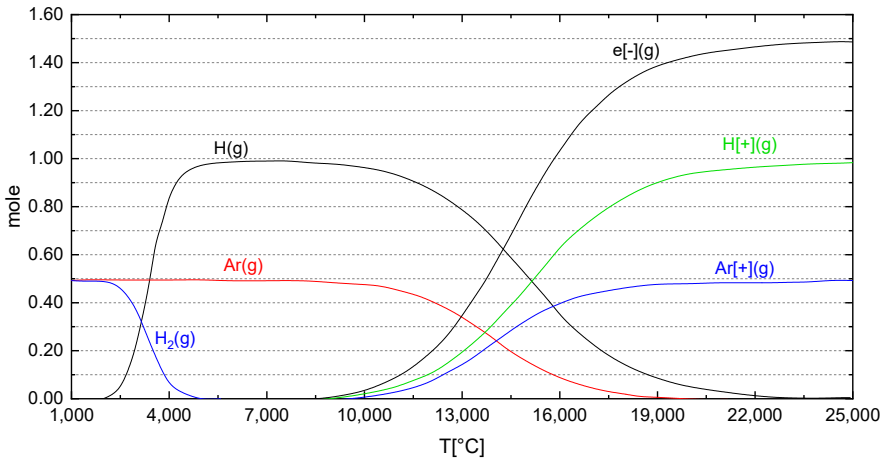

Figure 2. Gas composition of an H_2–Ar mixture over the temperature at 100 kPa (FactSage™ 7.1, Database; FactPS 2017) [14.]

As already mentioned, the diverse species of hydrogen are all different concerning their behavior during the reduction of metal oxides. Figure 3 shows different states of hydrogen and their activation barrier ($E_{1–4}$) for the reduction reaction in comparison [18]. For the comparison, the following order of activation energies (2–2) is valid. Ionized hydrogen is not mentioned because the amount is rather low in comparison to the other species under HPSR process conditions:

$$E_1 > E_2 > E_3 > E_4 \quad (2)$$

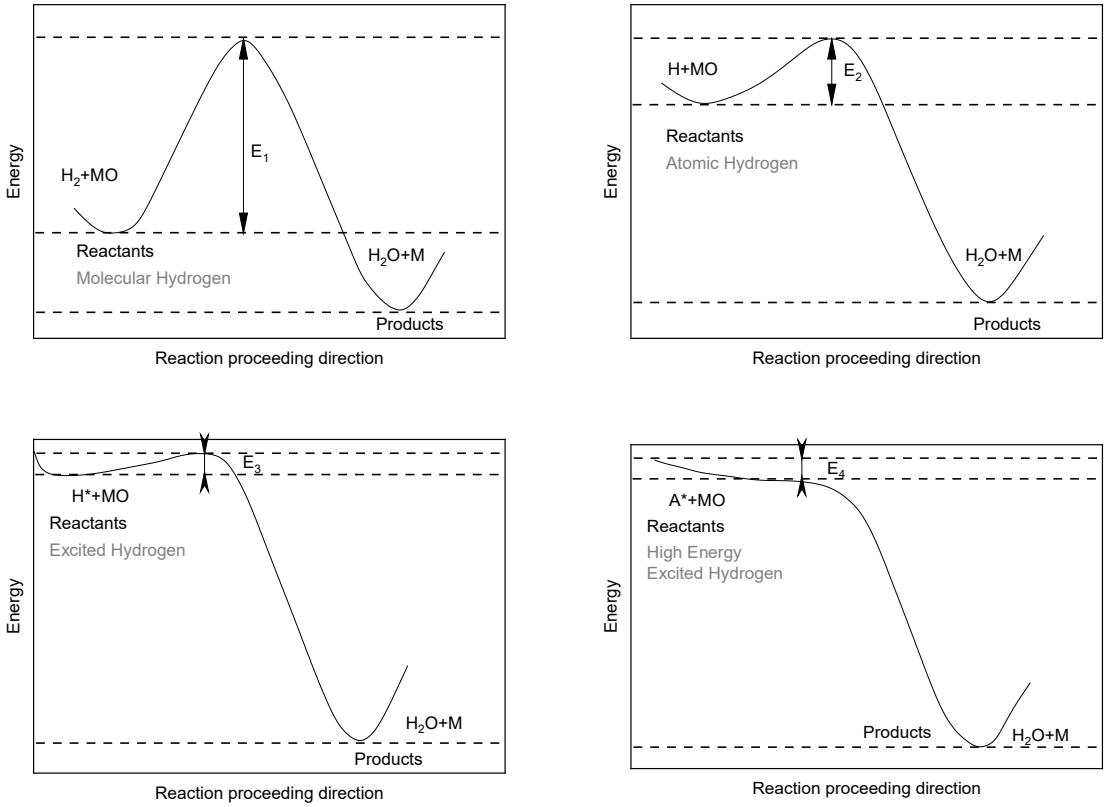

Figure 3. Schematic diagrams for the activation barriers for the different reduction of metal oxides by different hydrogen species [18].

The closer the hydrogen gets to its final ionized state (transition via the route in Equation (1)), the lower the activation energy of the process drops (transition via the route in Equation (2)), which is why it is crucial to reach a high amount of ionized hydrogen in the mixture to provide the best reduction conditions from a thermodynamic point of view. As well known, not only thermodynamics are important for the reduction behavior, but the kinetics of the process are also decisive. The kinetics of the process have already been discussed in previous works [11]. With the connection of thermodynamics and kinetics in mind, it is important to take a look at the next figure—Figure 4—to have a closer insight into the temperature distribution of an idle plasma arc in a tungsten welding process under argon [19]. This distribution is not quantitatively valid for the specifics of the HPSR process, but it still shows the principle for the following explanations.

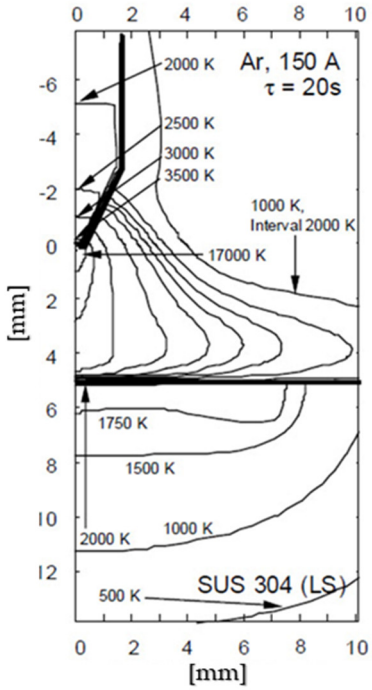

Figure 4. Simulation of the temperature distribution in an argon plasma flame using a tungsten electrode, operating at 150 A for 20 s [19].

If we consider the ionization behavior of hydrogen shown in Figure 2, a temperature of around 5000 °C was needed to reach the fully atomized state of hydrogen. Even a higher temperature of around 7500 °C is necessary to reach the ionized state. Considering these two temperatures, only the central area of the plasma arc can provide the energy required for ionization. Figure 5 illustrates a more likely position of the arc. It is characterized that the arc is not burning in the centerline of the electrode. It was shifted due to the uneven temperature distribution in the vicinity of the arc, the topography of the molten steel and slag as well as the electromagnetic forces. It can be seen that with a non-centered arc, the isothermals also shift. The negative consequence for the reduction is that the supplied gas and ore stream does not follow this shift. This means that at a certain point of dislocation, the required temperature for the atomization and ionization of the hydrogen is not reached and the iron ore particles are not completely melted inflight between the electrode tip and the melt. This can lead to a point where the economic feasibility of the process is at stake. Hence, the focus for future operations lies on the evaluation of the parameters for a stable centered burning arc.

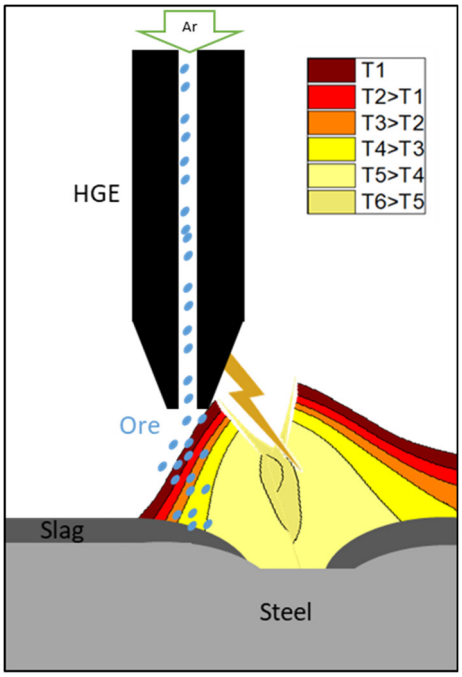

Figure 5. Schematic visualization of the effects of the arc shift between the hollow graphite electrode (HGE) and the steel bath on the thermal profile in hydrogen plasma smelting reduction (HPSR) processes.

2.2. The Importance of Arc Stability in the HPSR Process

The temperature distribution shown in Figure 4 is, as already mentioned, assumed for the idle state. As the practical work with plasma arcs indicates, there is nothing less likely than the idle state in the common operation. The most favorable conditions for arcs are the lower currents in the low arc gaps. Jones et al. [20] have shown that the increase in the arc current under steady conditions (constant gap in the air) leads to the chaotic and irregular motion of the arc. The arc geometry is not only influenced by the amount of power supplied; it was also influenced by the geometry of the cathode, the charged materials and gases, its movement while operating and the magnetic force field produced by the circuit. Due to these reasons and many others, it is more likely that the arc is not centered and has no idle evenly distributed temperature field. Figure 6 shows some of the much more likely positions of the arc during operation. Considering this arc drift, it was obvious that the conditions for the reduction are not at their best at all times. Figure 7 shows the movement of a DC arc with a high current flow, signifying a chaotic behavior [20].

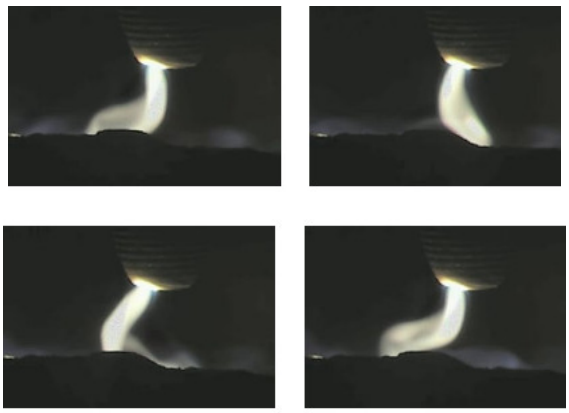

Figure 6. Some examples of the arc geometries in the air in a constant gap [20].

Figure 7. Example of the chaotic movement of the arc due to the increase in the arc current [20].

If the centered feeding of material through the hollow graphite electrode (HGE) in the HPSR process is taken into account, it is clear that only positions close to the idle state can provide the required temperature field of the arc in the right position of the introduction of the iron ore fines. In all other cases, the temperature field shifts towards the side of the electrode, and lower temperatures are reached in the ore introduction zone of the process. Consequently, the amount of excited and ionized hydrogen, and in combination, the productivity of the process, decreases. This decrease can be decisive for the economic efficiency of the process, which means that it is of the utmost importance to produce the most favorable conditions for its reduction and find the best conditions for a centered arc.

2.3. Aim of the Work Shown

The major point of this investigation was to define the possible parameters for a stable process. This means defining a field of stability for the variation of the gas compositions and the arc current and voltage supplied as well as the changes during the charging of iron ore. Regarding this study, the term stable is defined by the following parameters:

- The arc is burning for a timeframe of 10 s without any signs of instability;
- The arc has a minimum length of 20 mm;
- The arc is centered all the time (mainly important for longer arcs).

Centered means that the total deviation of the arc length is lower than the error values shown in Table 1, which are compared to a perfect straight downwards burning free arc.

Table 1. Absolute and relative errors concerning the idealized straight downwards burning arc.

Minimum arc Length at Perfect Conditions (mm)	Maximum Valid Arc Length (mm)	Absolute Error (mm)	Relative Error (%)
20	25.0	5.0	25.0
25	29.2	4.2	16.6
30	33.5	3.5	11.8
35	38.1	3.1	8.8
40	42.7	2.7	6.8
45	47.4	2.4	5.4

For a better understanding of the deviation definition, a sketch and the accompanying formulas are displayed in Figure 8.

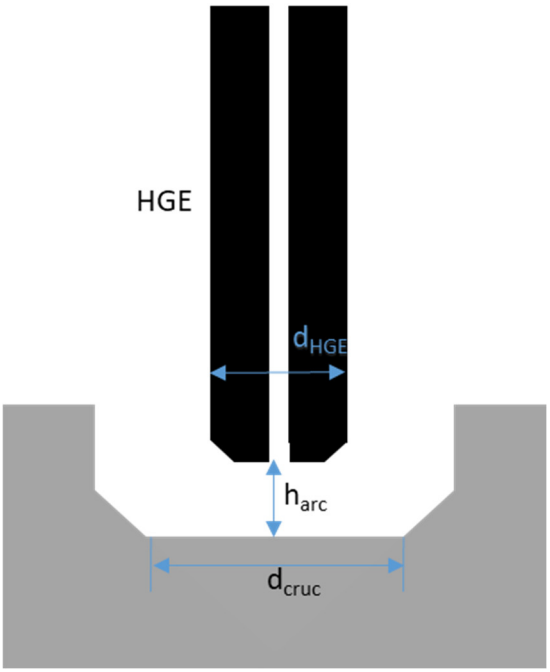

Figure 8. Schematic for the definition of the absolute and relative errors during the operation.

$$L_{max} = \sqrt{{h_{arc}}^2 + (\frac{1}{2} * d_{cruc} - \frac{1}{2} * d_{HGE})^2} \quad (3)$$

$$f_{abs} = L_{max} - h_{arc} \quad (4)$$

$$f_{rel} = \frac{L_{max} - h_{arc}}{h_{arc}} * 100 \quad (5)$$

L_{max}: Maximum valid arc length [mm]
h_{arc}: Minimum arc length under perfect conditions [mm]
d_{cruc}: Diameter of the crucible [mm]
d_{HGE}: Diameter of the HE [mm]
f_{abs}: Absolute error [mm]
f_{rel}: Relative error [%]

Under these conditions, so-called fields of stability are to be defined for various gas compositions and current levels. The final layout of such fields is already shown in Section 1—Figure 1.

3. Materials and Methods

3.1. HPSR Laboratory Equipment

For the trials, the HPSR facilities in the laboratory of Montanuniversitaet Leoben, Austria, were used. The facilities have been described in detail multiple times in previous works [15,21,22]. In Figure 9, the basic components of the reactor were shown. The arc was generated between the HE (1) and the ignition pin (3). The arc was a transferred DC arc with an average power input of ~5 kVA. The system was due to the implementation of an SCR power controller able to operate seamlessly in the range of 1–12 kVA. This range is of course not fully achievable for all gas compositions and arc lengths. More details concerning this will follow. The HGE has an inner diameter of 5 mm and an outer diameter of 26–30 mm. The outer diameter is not constant during a longer trial because some of the graphite is burned during the process. The loss of carbon during the trials is in the range of 1–3 g/h of operation. The constant conditions in these specific trials were evaluated over a timeframe of ~10 s. This means that despite the loss of graphite during the process, the rather low changes can be

neglected for the evaluation of the fields. The ignition pin (3) has a diameter of 10 mm and a height of 20 mm and is MIG welded to the crucible (4) in two spots in the intersection area. The crucible has an outer diameter of 100 mm, a height of 25 mm and can carry up to 100 g of ore at the start of the trial if the trial is operated in batch mode. The diameter of the flat base of the crucible is 54 mm. Those 54 mm are important for the explanation of the deviation in arc lengths. In some trials, the material was introduced at charging rates of ~3 g/min with the gas through the HGE. For this operation, a powder dosing system from LAMBDA Laboratory Instruments (Figure 10) was used. Argon and hydrogen were injected through the HGE into the arc zone to create ionized species. In trials without iron ore fines, nitrogen was also mixed with either hydrogen or argon to define a wide variety of stability fields. A refractory ring (2) to protect the bottom disc in case of a meltdown of the inclined crucible wall enclosed the steel crucible. These meltdowns only occur when the arc is not centered anymore, so the optical inspection of the crucible after the trial could tell if the arc was shifting from the center of the system at any point in time. Additionally, the process was under surveillance by a camera system to ensure a permanently stable behavior.

1- Hollow graphite electrode (HGE)
2- Refractory ring
3- Ignition pin
4- Steel crucible
5- Bottom electrode
6- Refractories
7- Electrode holder with the cooling system
8- Four orifices to (a) install off-gas duct, (b) monitor the arc, (c) install a pressure gauge and (d) install a lateral hydrogen lance
9- Reactor roof with refractories and cooling copper pipes
10- Steel pipe to inject gases and the continuous feeding of fine ores
11- Viewport used for the camera system

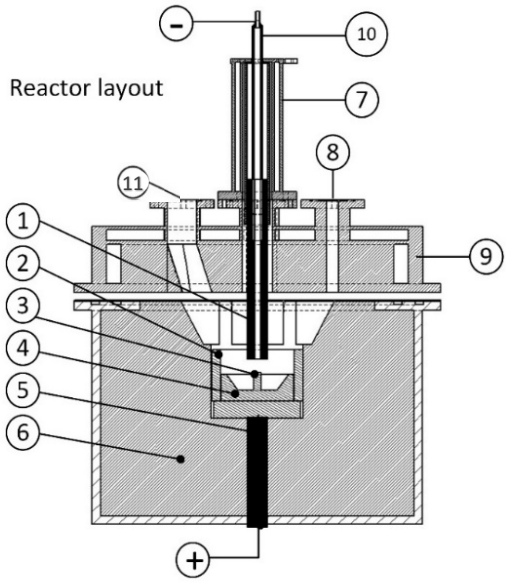

Figure 9. Reactor layout and list of the most important components reproduced from Reference [15] with permission.

Figure 10. Hi-Doser 0.2l, powder-dosing instrument.

The charging system consists of a dosing unit and a powder distributor coupled to a stepping motor that controls the rotations per minute and the charging rate, accordingly. For the analysis of the off-gas, a mass spectrometer (MS) from Pfeiffer Vacuum Technologies, Vienna, Austria (Type GAM200) was used. For the analysis, the gas was led through an off-gas cleaning system where the gas got de-dusted and de-humidified. The de-dusting was done in a three-step process where at first,

the gas was led through a mineral wool filter, after which it was fed through two bottles of 1 L water mixed with a substance to decrease the wetting angle of the carbon particles dispersed in the gas for a better dissolution. This was done because the fine carbon particles filtered by the water would float on the surface without any additives. Due to the emerging gas-bubbles on the surface, the swimming carbon can be picked up again in the gas phase and surpass the system that is meant to absorb it. For the final de-dusting, the gas was conveyed through two columns containing mineral wool for the separation of the remaining particles. After this de-dusting step, the gas surpasses two columns of molecular sieves for de-humidification. The last column of the gas cleaning system was filled with silica gel to indicate if the gas was fully de-humidified and de-dusted. Due to a possible layer of carbon or the change in color of the gel pearls, it was easy to indicate if the system worked as planned or if the load of dust and humidity was too high for the system.

A simplified version of the facility's circuit diagram is shown in Figure 11. The ampere meter shown is an LEM, Schwechat, Austria HTA 200-S Hall sensor system operating in the range of 0–300 A ± 1%. The volt measurement was done by an APM-VOLT-APO digital meter from Truemeter, Bury, Lancashire, UK that operates at a relative precision of ± 1%.

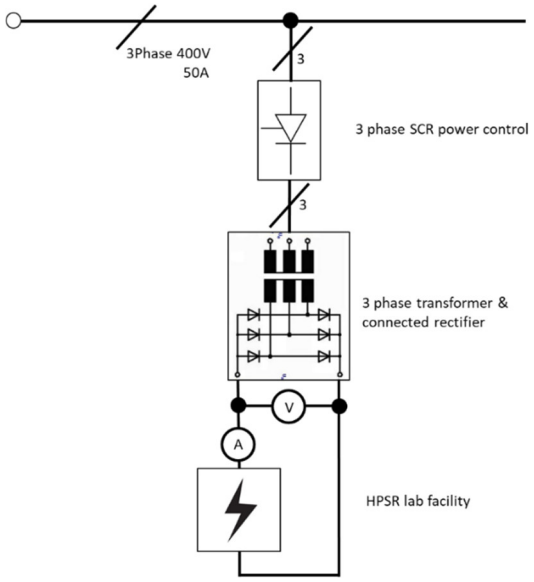

Figure 11. The simple circuit diagram with the use of a silicon-controlled rectifier (SCR) and the positions of measurement for the HPSR lab facility.

For the observation of the arc, the camera system Axis-Q1775 from Pieper GMBH, Schwerte, Germany was used. The standard camera was configured with two additional filters. The first filter is an IR filter type FRO7012 from Pieper GMBH for furnace chamber observations with a thickness of 2 mm. The second filter was a gold-plated disc from Pieper GMBH with 30% remaining permeability and a thickness of 2.5 mm. Figure 12 shows the standard configured camera and the adjustment of the camera system on the lid of the furnace. The orifice shown is the viewport (11) in Figure 9.

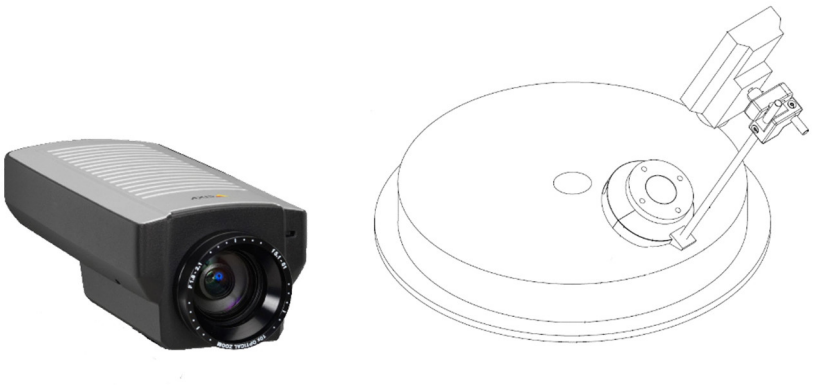

Figure 12. Camera system and a sketch of the mounting on the lid of the HPSR lab reactor.

For the controlled supply of the gas components hydrogen, argon and nitrogen, mass flow controllers type EL-FLOW PRESTIGE FG from Bronkhorst High-tech B.V, AK Ruurlo, Netherlands were utilized. The specifications are listed in Table 2**.** For all trials, the gas qualities listed in Table 3 were used.

Table 2. Type and operation range of EL-FLOW PRESTIGE FG flow controllers.

	Type	Range (Nl/min)
H_2	F-201C-FAC-22-E	0–10
Ar	F-201CV-10K-AAD-33-V	0–10
N_2	F-201CV-20K-AAD-33-V	0–20

Table 3. Qualities of the gases used for the trials.

Gas	Purity	Remarks
H_2	5.0	–
Ar	5.0	O_2, N_2, $H_2O \leq 5$ppm
N_2	5.0	O_2, $H_2O \leq 5$ppm

3.2. Experimental Program and Materials

In the present study, multiple series of experiments were designed to study the fields of stability for the HPSR process. The program is shown in Table 4. The experiments were accumulated in 22 sets within three groups. In these sets, the power level of the transformer (column 2), the gas mixture (column 3), the maximum current flow (column 4) and the arc length (column 5) were varied. For the variation of the current, the level of the PCR power controls potentiometer was listed instead of a fixed amperage value. The exact definition of a fixed current was not possible due to the circuit design. In the last column, the operation mode was listed. Two modes (pure steel/continuous feed) were applied and the trials were classified into three groups.

Set Grp 1. Single gases and mixtures of argon and hydrogen;
Set Grp 2. Single gases and mixtures of argon and nitrogen;
Set Grp 3. Single gases and mixtures of nitrogen and hydrogen.

The total flow rate for all experiments was kept constant at 5 Nl/min. The facility was operated at two different power levels. The first one operated at around 90–100 A and provided a power output of up to 9 kVA, while the second one provided 15 kVA with a current at around 150–160 A.

Table 4. Experimental table for the evaluation of the arc stability fields.

Number of exp. set grp 1	Power level (1/2)	Hydrogen in argon (%)	Variation of current (% of I_{max})	Variation of arc length (mm)	Charging of 3 g/min iron ore
1	1	0	60–100	20–45	steel
2	1	10	70–100	20–45	steel
3	1	20	70–100	20–45	steel
4	1	30	80–100	20–45	steel
5	1	40	80–100	20–45	steel
6	1	40	85–100	20–45	continuous
7	2	0	60–100	20–45	steel
8	2	10	70–100	20–45	steel
9	2	20	70–100	20–45	steel
10	2	30	75–100	20–45	steel
11	2	40	75–100	20–45	steel
12	2	40	80–100	20–45	continuous
Number of exp. set grp 2	**Power level (1/2)**	**Nitrogen in argon (%)**	**Variation of current (% of Imax)**	**Variation of arc length (mm)**	**Charging of 3 g/min iron ore**
13	1	0%	60–100%	20–45	steel
14	1	50%	70–100%	20–45	steel
15	1	100%	75–100%	20–45	steel
16	2	0%	60–100%	20–45	steel
17	2	50%	70–100%	20–45	steel
18	2	100%	75–100%	20–45	steel
Number of exp. set grp 3	**Power level (1/2)**	**Hydrogen in nitrogen (%)**	**Variation of current (% of Imax)**	**Variation of arc length (mm)**	**Charging of 3 g/min iron ore**
19	1	0%	75–100%	20–45	steel
20	1	40%	85–100%	20–45	steel
21	2	0%	75–100%	20–45	steel
22	2	40%	80–100%	20–45	steel

Similar to the previous studies [8,9,11–14], Carajas hematite iron ore was used for the experiments. The composition of the most important elements and the share of bivalent and trivalent iron are listed in Table 5. The grain size distribution of the iron ore is shown in Table 6. Table 7 contains the chemical composition of the steel crucible and the steel pin material.

Table 5. Chemical composition of the iron ore.

No	Element	(wt.%)
1	Fe_2O_3 [1]	92.83
2	FeO	1.07
3	Total Fe	65.81
4	Silica	1.694
5	Aluminum oxide	1.01
6	Manganese	0.17
7	Phosphorus	0.057
8	Total sulfur	0.014
9	LOI [2]	2.79

[1] Calculated value after analysis, [2] Loss of ignition

Table 6. The grain size distribution of the Carajas iron ore.

Mesh Size (μm)	Fraction (wt.%)	Cum (wt.%)
63–125	50	50
25–63	50	100

Table 7. Chemical composition of the ignition pin and steel crucible [23].

Element	Unit	C	Si	Mn	P	S	Cr	Mo	Ni	Al	Cu
Steel crucible	(wt.%)	0.178	0.261	1.325	0.009	0.005	0.083	0.031	0.168	0.027	0.179
Ignition pin	(wt.%)	0.441	0.217	0.85	0.008	0.028	0.985	0.162	0.085	0.021	0.116

3.3. Description of the Operation

Before the start of each series of trials, the steel pin of the crucible was pre-melted and after completion, the operation was stopped. Subsequently, the molten pool solidified and the electrode was set to the contact position. In this position, the level indicator of the electrode positioner was set to zero. This had to be done because of the changes in the surface pattern and the length of the electrode in between the trials. After the meltdown of the pin and the zero level set, every trial was started under a pure argon atmosphere. Following the ignition of the arc, the electrode was raised to a height of 20 mm. From this stage onwards, the individual setups were adjusted. The voltage and amperage were measured continuously throughout the whole trial.

Example of the Operation in the Case of Group 1 Set 2 (10% Hydrogen in Argon at Variations of Arc Length and Supplied Current)

The trials of set 2 started at 20 mm height and a stable arc for a timeframe of 10 s. After that, the conditions were changed to 10 %-vol. H_2/90 %-vol. Ar and the arc length was adjusted to the evaluated level (20, 25, 30, etc. mm). At a fixed length and gas composition, the current was steadily decreased with a potentiometer which was connected to the SCR power controller. This operation was carried out until the arc disconnected, or for some trials until the limit of stability was already reached at a level above the point of disconnection. This was the case when the arc was not centered anymore according to the limit defined in Section 2.3. This procedure was applied for all sets of trials (1–22) to evaluate the limits of stability.

3.4. Methods for the Evaluation

The limiting values of current and voltage were evaluated and graphically presented in two ways.

1. Arc stability maps;
2. Fields of stability.

To get this kind of diagram, the curves of the voltage and amperage measured were evaluated for the varying conditions that were designated as stable. Figure 13 shows such a measurement. The figure shows, besides the blue-dotted and red line-dotted curve for current and voltage, some green-crossed indicators. These values are the discarded voltage values for the evaluation. They were discarded because they did not comply with the defined stable parameters.

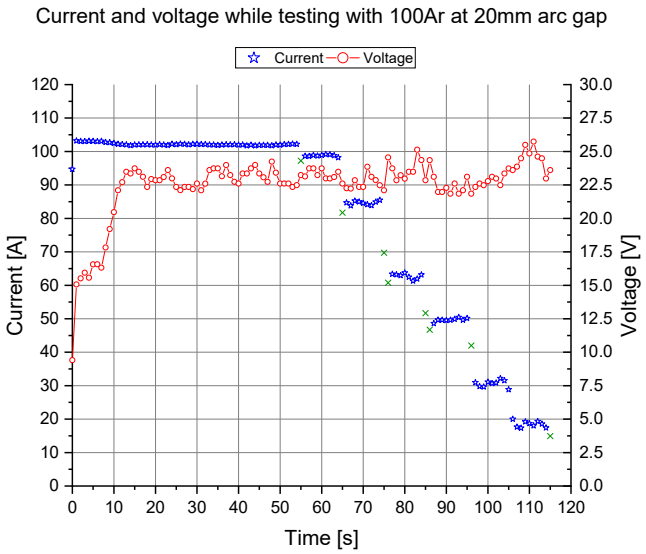

Figure 13. Measurement for the first series of trials in set 1. Pure argon 20 mm arc gap in the idle centered position.

Figure 14 shows the arc in different positions during the validation. For a better understanding of the picture, the contour of the HGE (black), the basic diameter of the crucible, which shows the stable area (dotted), and the center of the arc (dash-dotted) are marked additionally.

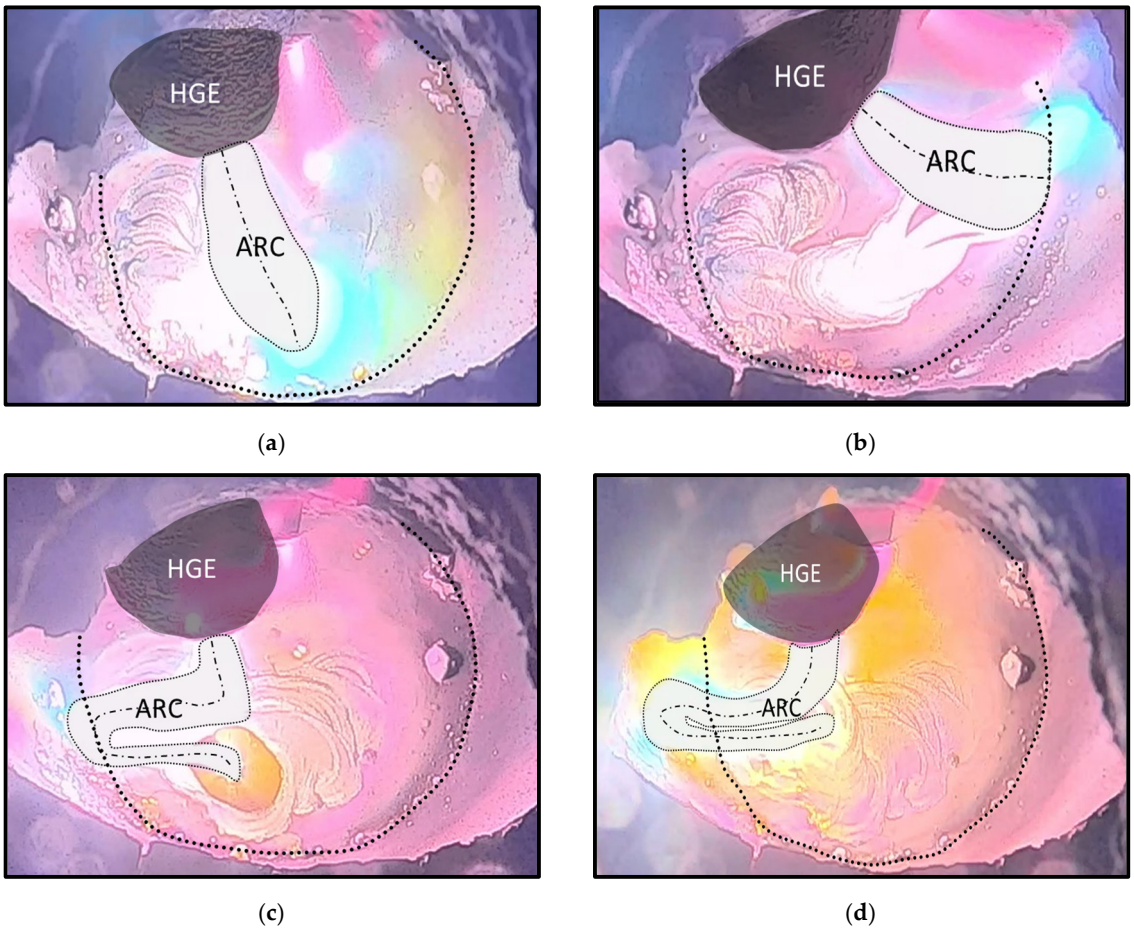

Figure 14. Different positions for the arc during operation: (**a**) stable centered position; (**b**) position at the operation limit; (**c**) invalid position and signs of instability; and (**d**) invalid position, and chaotic behavior.

In Figure 14a, a straight downwards burning arc is shown. Figure 14b shows an arc touching the basic diameter of the crucible and its position is at the outer limit of the region defined as stable. In Figure 14c, the arc already crossed the region of stability and shows signs of instability. In the fourth Figure 14d, the arc shows a very unstable behavior and the position is far away from the defined stability boundaries.

3.4.1. Arc Stability Maps

Within the arc stability maps, all the trial limits are presented. Table 8 shows an example of such a map with 100% argon at power level 1 with no added ore.

Table 8. Example of an arc stability map.

SET 1 100% Ar PL 1		SCR level of potentiometer [%]								
		100	95	90	85	80	75	70	65	60
L_{arc} [mm]	20									
	25									
	30									
	35									
	40									
	45									

The set number, gas composition and applied power level are indicated in the top left corner. Throughout the rows, the decrease in the electric current is visualized via the levels of the potentiometer and in the columns, the height of the arc is shown, which is directly connected to the voltage drop in the arc zone. For the indexing of the squares, four different colors for the following categories were applied:

1. **Green:** clearly stable;
2. **Petrol:** showed stable behavior, but can be unstable under certain circumstances;
3. **Orange:** showed unstable behavior, but can be stable under certain circumstances;
4. **Red:** clearly unstable or extinguished.

For a better understanding of the area definition, the four different categories were explained in detail in the following section. Especially for the petrol and orange areas, the behavior of the arc and the stability definition in Figure 8 (possible change in length between L_{max} and h_{arc}) are important points.

Ad1 (green)

The green areas indicate an area of definite stability. This means that the arc was either at no point close to disconnection or the outer region (close to the dotted line) of the area was defined as stable. Additionally, slight changes in height or a lower amount of supplied power would not change this circumstance.

Ad2 (petrol)

The arc mainly connects at the border of the molten pool and the solid adjacent material. This happens due to the point effect of the electrical field at the sharp edge at the interface of the pool and the solid material. Because of this, the solid material at the edge starts to melt due to the transferred power, and the molten pool therefore changes its position. If the power input is high enough, the pool increases in size. At a certain size of the pool, the arc starts to shift from the edge of the pool to the center of the molten material. This happens because the arc length on the outer border of the pool is too close to L_{max} and this leads to a less stable arc compared to the direct connection towards the

center of the melt. This phenomenon could occur in two ways; in the first case, if the pool is centered in the crucible, the arc is always shorter than the aforementioned L_{max} of the stability definition. Therefore, the arc seems more stable at longer adjusted arc lengths, meaning that with a centered pool, the experiment may seem more stable. The second case is relevant if the pool is out of the centerline of the electrode. Due to this, the opposite effect could occur and the length of the arc would be closer to L_{max} than to h_{arc} at all times. In this situation, the arc seems less stable. Both cases are possible, so the areas are marked as petrol because the stability depends on the position of the molten pool.

Ad3 (orange)

If the power input is decreased below a certain level, the minimum energy for the further liquefication of the material cannot be reached anymore. This means the liquid pool decreases in size until it reaches a certain minimum. At this point, the arc tends to "jump" towards other locations. This location can be further away from the center, signifying that the arc is more likely in a position where the arc length is closer to L_{max}. The arc in the experiment may have seemed unstable, but it was simply connected to the anode at longer distances and lost its connection earlier as a result.

Ad4 (red)

The red areas indicated an area of definite instability. This means that the arc was either disconnected or clearly out of the defined stable region. Additionally, slight changes in height or a higher amount of supplied power would not have changed this circumstance.

3.4.2. Fields of Stability

For the fields of stability, the stable conditions are presented in a voltage via amperage diagram (Figure 15). For all evaluated points, the deviation during the measurement was evaluated and presented via error bars. The trials are not grouped in the first-mentioned sets anymore. All the data were regrouped by their gas compositions (e.g., in Figure 15 100% N_2). This meant that the field of 100% N_2 shown was created from the data from sets 15, 18, 19, 21 out of Table 4. For these fields, all the data of both power levels were also combined to present one final diagram for the direct comparison of the fields of stability as a function of the gas composition. In other words, each gas composition is presented in varying colors and symbols. A correlation among these data points is difficult to visualize. For this reason, all of the stable points measured are framed in the matching color of one specific gas composition in a second diagram. For better visualization, the error bars are hidden in this graph. This second graph defines the field of stability for a specific gas composition under various conditions, as introduced in Figure 1.

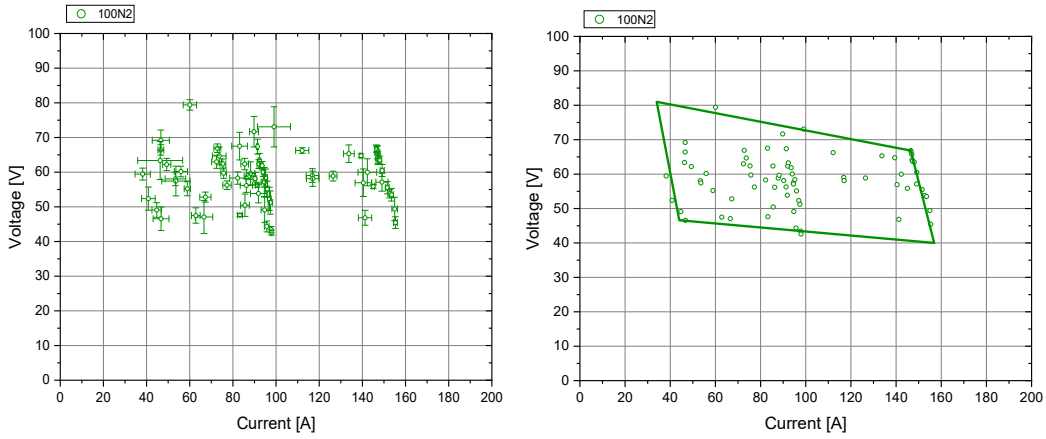

Figure 15. Example of the evaluation of the field of stability for 100% nitrogen.

4. Results and Discussion

In the following tables, the results of the fields chosen are presented to show the most important data for the following discussion.

4.1. Arc Stability Maps

The arc stability map collection in Table 9 presents the change in the fields while increasing the hydrogen concentration. The final pair of charts shows the influence due to the introduction of ore through the HGE.

Table 9. Collection of arc stability maps for various conditions in the HPSR process for single gases and mixtures of argon and hydrogen.

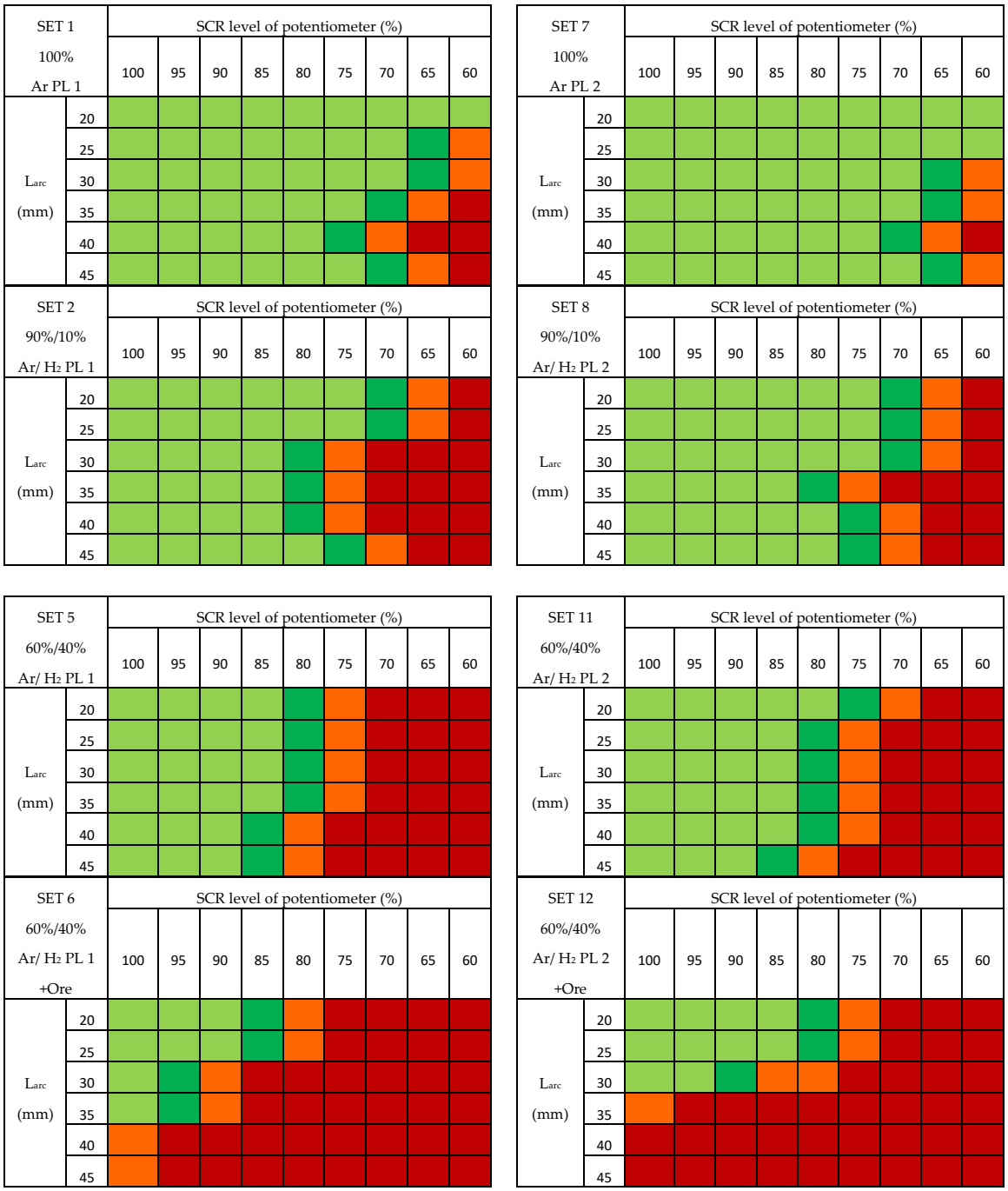

It can be seen that the higher the concentration of hydrogen is, the smaller the field of valid parameters becomes for a stable arc. Moreover, from left to right, a trend in higher levels of stability is shown due to the increase in the available power input. In the last two maps, the influence of ore charging is visualized. It clearly shows a drastic decrease in stability due to the effect of the charging of ore. This means that in the full-scale process, the field of stability is the smallest, and so it is very

important to evaluate these parameters to ensure the best kinetic and thermodynamic circumstances for the process.

Furthermore, a trend of lower stabilities at midrange arc lengths is observable. Table 10 shows the described trend (arrows) as an example for set 2. This trend is mainly observable at arc stability maps with a wider area of stability, meaning lower hydrogen/nitrogen and higher argon contents without the charging of ore. In these areas, the increase in the voltage per arc length is lower than in those with a lower argon gas content. This means that the arc can shift for very short periods towards the wall of the crucible without disconnecting. Moreover, a wider area of the stable position is realizable due to the sufficient level of power, meaning that the absolute error can be realized at its full length. At higher arc lengths and lower currents, the arc is unable to shift in the total range defined as stable; due to a lack of power supplied, the arc centers itself and seems to be more stable at higher arc lengths. This effect only occurs due to the stability definition and is not connected to any special physical phenomenon, as the following visualization via the stability fields will show.

Table 10. The trend of lower stabilities at mid-range arc lengths.

SET 2 90%/10% Ar/ H_2 PL 1		SCR level of potentiometer [%]								
		100	95	90	85	80	75	70	65	60
L_{arc} [mm]	20									
	25									
	30									
	35									
	40									
	45									

4.2. Fields of Stability

For the following graphs, the method for arc stability fields (Section 3.4.2) was used. Additionally, lines of equal power input are shown in the chart to obtain a better understanding of the data. Figure 16 shows the comparison of fields with different gas compositions. It can be seen that pure argon shows the most stable behavior of all the gas compositions tested. This is indicated due to the wide range of realizable currents (width in x axis) and the low increase in voltage by arc length (height in the y axis) of the stability field. In comparison to pure argon, pure nitrogen already starts at a higher base level of voltage for a length of 20 mm. Additionally, it increases at a higher value per millimeter of arc length, so the field is wider and higher. Measuring a field for pure hydrogen was not possible because the power supply could not provide sufficient power. For that reason, only mixtures of argon and hydrogen were compared to the pure gases. The gas mixture of argon and nitrogen situates itself—as predicted—right in the middle of the fields of the pure gases. Taking into account that this is a valid assumption for all gas mixtures, it is suggested that the field of stability for pure hydrogen would be in the region of 150 V–200 V and at a minimum amperage of 100 A.

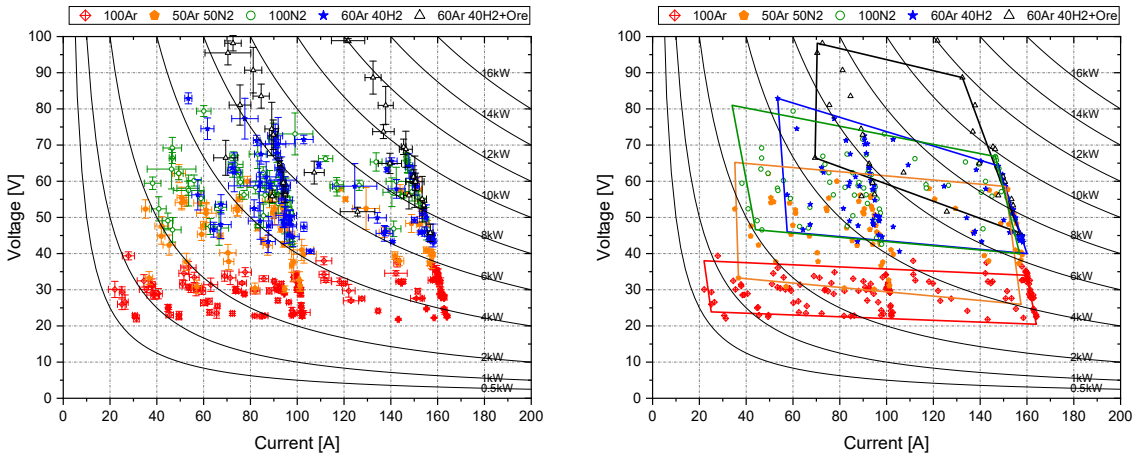

Figure 16. Arc stability fields for the variation of the gas composition and the effect of iron ore introduction via the HGE.

Figure 17 shows the change in the stability fields with increasing hydrogen concentration. The first trend that can be detected is the increasing base level of voltage with the increase in hydrogen. This means the x baseline of the frame shifts towards higher voltage levels. The second indicates that the fields increase in height (voltage per length) at increasing hydrogen concentrations. It was also observable that the charging of 3 g/min of ore fines leads to reaching the limit of the power supply in certain regions of lower currents (~80 A). In this figure, only the highest realizable amount of hydrogen (40% in 60% argon) in connection with the charging of ore is shown. This is for two reasons, the first of which is to keep the diagram at a readable state. The second is that this mixture is of high interest because the specific hydrogen flow is adjusted to the amount of ore charged. The conditions for the reaction are always at the best ratio of hydrogen to oxygen charged from the ore for the reduction.

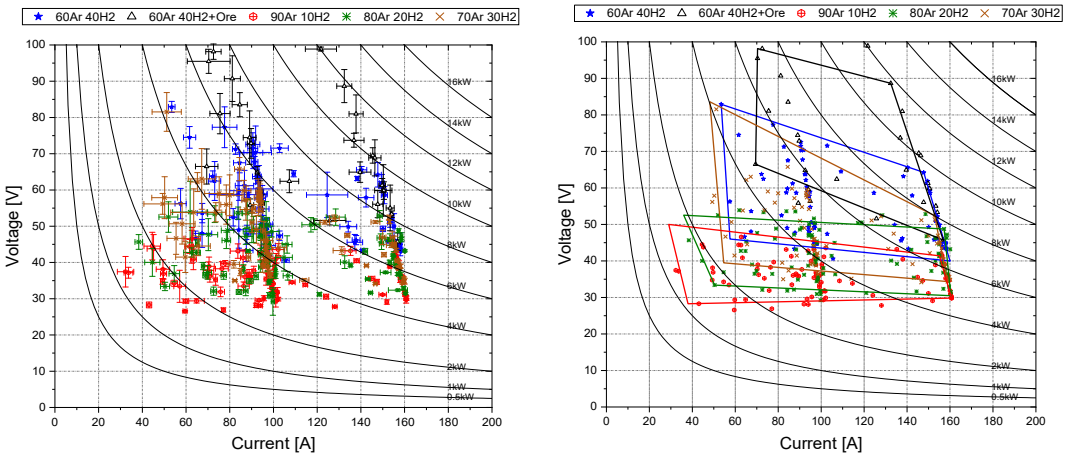

Figure 17. Arc stability fields for the variation of the hydrogen content and the effect of iron ore introduction through the HGE.

In the comparison of Figures 16 and 17, they show three major patterns of similar behavior. First, the fields tend to get narrower with an increase in the base level of voltage. For example, the base level of pure argon is in the region of 20 V–25 V; at this low base level, it is possible to reach currents of below 30 A with a stable arc. If this is compared to pure nitrogen, which has a base level from 40 V to 45 V, stable arcs can only be achieved at 38 A and above. Second, the fields tend to increase in their voltage per distance value of the arc at a decreasing level of argon. Table 11 shows this trend. It is also easy to see this phenomenon in the figure by the fact that the higher the x-baseline of the frame

of the gas starts, the higher the fields get. Third, at higher power input levels and the stages closer to the low power boundaries of stability, the error bars of the values tend to increase. This seems to be because the power supply reaches its limits in these regions.

Considering the up-scaling of the technology, only two additional major findings could be stated. The first is the possibility to control the power input by adjusting the gas composition. The lower the argon content in the gas mixture with hydrogen is, the higher is the power input. The lab facilities' trials show a change in the power input by a factor of 8 when using 40% hydrogen in the mixture in comparison to pure argon. The second finding is the increase in the voltage drop in the arc zone by an increase in the nitrogen or hydrogen content. This can be explained by the higher ionization energy for two atomic gas molecules. This is an important finding for the scale-up of the technology, because the maximum voltage drop in the arc is a design criteria of the electric power supply.

Table 11. Change in voltage per centimeter of arc height for mixtures of argon and hydrogen in comparison to pure argon.

	100% Ar	**90% Ar 10% H_2**	**80 %Ar 20% H_2**	**70% Ar 30% H_2**	**60% Ar 40% H_2**
ΔU (V/cm)	1.0–6.0	2.1–5.2	4.2–8.6	4.5–10.5	6.2–10.3

5. Conclusion and Outlook

The present study investigated the behavior of the transferred DC arc in the HPSR process. The HPSR process is a smelting reduction process for the direct production of steel out of iron ore in a CO_2 emission-free one-step process. The result is the presentation of the evaluated data in so-called arc stability maps and fields of arc stability. These diagrams can be used not only for the design of further trials in the ongoing investigation, but also for the scale-up of future facilities. If the next step in the development of such fields and maps shows that there is a correlation between the fields of smaller and bigger production facilities, the process will take a huge step towards its industrial application.

5.1. Conclusion

The investigation was done by measuring the arc voltage and current during the change of system parameters' gas composition, arc length, the addition of ore to the gas stream, and the limitation of the current flow of the power supply by the implementation of an SCR power controller. All the measurements were filmed during the operation and evaluated visually for their validity in certain defined fields of stable arc parameters. As a result, the data evaluated were converted to so-called fields of stability and arc stability maps to visualize the data. Regarding the visualization via the diagrams and the evaluation of the filmed pictures, the following conclusions could be made:

- The comparison of the different fields shows that the maximum realizable power input is also limited by the gas composition;
- Argon is the most stable gas and acts as a stabilizer in gas mixtures, but with the addition of argon, the maximum transferrable power is also limited;
- With increasing hydrogen, the field shifts towards higher levels of minimum voltage (shift of the frame towards the top right);
- With increasing hydrogen, the fields tend to increase in voltage per mm of arch length (higher y axis spread of the frame);
- Lower levels of amperage are not reachable at higher levels of voltage (shift of the low current border of the frame towards the top right of the diagram);
- Mixtures of gases position themselves in the middle of the surrounding pure gas stability fields;
- If this assumption is true for all mixtures, pure hydrogen would have its baseline at around 150 V–200 V and need a minimum amperage of around 100 A;
- The charging of ore decreases the stability drastically (harsh shift towards the upper right corner of the frame);

- The limits for charging and the amount of hydrogen in argon need to be adjusted to find the perfect ratio for the available hydrogen and the oxygen input through the iron ore;
- The error bars for the results produced increase with increasing instability of the arc;
- The error bars also tend to increase their value the closer the system gets to its maximum power level;
- The increasing amount of hydrogen in the mixture with argon leads to an increase in the supplied power by the factor of 8 in the investigated range of 0–40% hydrogen;
- The voltage drop in the arc zone increases with a raising hydrogen content in the mixture with argon. Therefore, a higher voltage level from the electrical power supply was needed at higher hydrogen content.

5.2. Outlook

These measurements and conclusions are only another small step towards the industrialization of the HPSR process. As already mentioned in the introduction, the evaluation of the voltage data during the trials was also a very important factor to define stable arc conditions even better with an assisted arc stability index (ASI) value. This value should focus on the one hand on the maximum deviation of voltage during a constant parameter setup in the process and on the other hand, on the change in voltage related to time (dU/dt) in this certain timeframe of constancy. Another important investigation is about to be conducted in the field of reduction parameters. The relation of stable arc conditions and the connected change in the reduction rate should especially be investigated. With the combination of ASI, stability fields, stability maps and the evaluation of the reduction parameters in the most stable regions of the former, a final setup for the comparison and correlation of the lab facilities and the bench-scale facilities should be establishable.

Author Contributions: Conceptualization, M.A.Z. and J.S.; methodology, M.A.Z.; validation, M.A.Z. formal analysis, M.A.Z.; investigation, M.A.Z. and M.A.F.; resources, M.A.Z.; data curation, M.A.Z.; writing—original draft preparation, M.A.Z.; writing—review and editing, J.S.; visualization, M.A.Z.; supervision, J.S.; project administration, J.S.; funding acquisition, J.S. All authors have read and agreed to the published version of the manuscript.

Funding: This research was funded by The Austrian Research Promotion Agency (FFG) with the project SuSteel, project number 853393, and the COMET program, K1-MET project number 869295. In addition, this research work was partially financed by the industrial partners voestalpine Stahl GmbH and voestalpine Stahl Donawitz GmbH and the scientific partner Montanuniversität Leoben.

Acknowledgments: The authors gratefully acknowledge the funding of the SuSteel project by The Austrian Research Promotion Agency (FFG) and the funding support of K1-MET GmbH, metallurgical competence center. The research program of the K1-MET competence center is supported by COMET (Competence Center for Excellent Technologies), the Austrian program for competence centers. COMET is funded by the Federal Ministry for Climate Action, Environment, Energy, Mobility, Innovation and Technology, the Federal Ministry for Digital and Economic Affairs, the provinces of Upper Austria, Tyrol, and Styria, and the Styrian Business Promotion Agency (SFG).

Conflicts of Interest: The authors declare no conflict of interest.

References

1. World Steel Association. Steel's Contribution to a Low Carbon Future and Climate Resilient Societies. Worldsteel Position Paper. 2020. Available online: https://www.worldsteel.org/en/dam/jcr:7ec64bc1-c51c-439b-84b8-94496686b8c6/Position_paper_climate_2020_vfinal.pdf (accessed on 9 October 2020).
2. Le Quéré, C.; Jackson, R.B.; Jones, M.W.; Smith, A.J.P.; Abernethy, S.; Andrew, R.M.; De-Gol, A.J.; Willis, D.R.; Shan, Y.; Canadell, J.G.; et al. Temporary reduction in daily global CO_2 emissions during the COVID-19 forced confinement. *Nat. Clim. Chang.* **2020**, 10, 647–653
3. Eurofer European Steel Association. *Low Carbon Roadmap: Pathways to a CO_2- Neutral European Steel Industry*; Final Report; EUROFER: Brussels, Belgium, 2019; pp. 1–18.

4. Energy Transitions Commission. Reaching Zero Carbon Emissions from Steel. Available online: http://energy-transitions.org/sites/default/files/ETC_Consultation_Paper_-_Steel.pdf (accessed on 15 July 2020).
5. Bäck, E.; Schenk, J.; Badr, K.; Sormann, A.; Plaul, J.F. Wasserstoff als Reduktionsmittel für die Eisen- und Rohstahlerzeugung–Ist-Situation, Potentiale und Herausforderungen. *BHM Berg- und Hüttenmännische Mon.* **2015**, 160, 96–102.
6. Sormann, A. Untersuchung zur Schmelzreduktion von Eisenoxiden mit Wasserstoff als Reduktionsmittel. Ph.D. Thesis. Montanuniversität, Leoben, Leoben, Austria, 1992.
7. Bäck, E. Schmelzreduktion von Eisenoxiden mit Argon-Wasserstoff-Plasma. Ph.D. Thesis, Montanuniversität, Leoben, Leoben, Austria, 1998.
8. Plaul. J.F. Schmelzreduktion von Hämatitischen Feinerzen im Wasserstoff-Argon-Plasma. Ph.D. Thesis, Montanuniversität, Leoben, Leoben, Austria, 2005.
9. Badr, K. Smelting of Iron Oxides Using Hydrogen Based Plasmas. Ph.D Thesis, Montanuniversität, Leoben, Leoben, Austria, 2007.
10. Goldston, R.J.; Rutherford, P.H. *Introduction to Plasma Physics*, 1st ed.; Institute of Physics Publishing: Bristol, UK, 1995.
11. Naseri Seftejani, M.; Schenk, J. Reaction kinetics of molten iron oxides reduction using hydrogen. *La Met. Ital.* **2018**, 7/8, 5–14.
12. Naseri Seftejani, M.; Schenk, J. *Thermodynamic Aspects of Hydrogen Plasma Smelting Reduction of Iron Oxides*; ICSTI: Vienna, Austria, 2018.
13. Naseri Seftejani, M.; Schenk, J. Thermodynamic of Liquid Iron Ore Reduction by Hydrogen Thermal Plasma. *Metals* **2018**, 8, 1051, doi:10.3390/met8121051.
14. Naseri Seftejani, M.; Schenk, J. *Transport Properties of HPSR Gases*; The Chinese Society for Metals (CSM): Beijing, China, 2018.
15. Naseri Seftejani, M.; Schenk, J.; Zarl, M. Reduction of Haematite Using Hydrogen Thermal Plasma. *Materials* **2019**, *12*, 1608.
16. Naseri Seftejani, M.; Schenk, J. Fundamentals of Hydrogen Plasma Smelting Reduction (HPSR) of Iron Oxides, A New Generation of Steelmaking Processes. In Proceedings of the 7th Asia Steel International Conference 2018, Odisha, India, 6–9 February 2018.
17. Sabat, K.C.; Murphy, A.B. Hydrogen Plasma Processing of Iron Ore. *Metall. Mater. Trans. B* **2017**, 48, 1561–1594.
18. Sabat, K.; Rajput, P.; Paramguru, R.; Bhoi, B.; Mishra, B. Reduction of Oxide Minerals by Hydrogen Plasma: An Overview. *Plasma Chem. Plasma Process.* **2014**, 34, 1–23.
19. Tanaka, M.; Ushio, M.; Lowke, J.J. Numerical study of gas tungsten arc plasma with anode melting. *Vacuum* **2004**, 73, 381–389.
20. Jones, R.; Reynolds, Q.; Curr, T.R.; Sager, D. Some myths about DC arc furnaces. *J. S. Afr. Inst. Min. Metall.* 2011, 111, 665–674.
21. Sormann, A.; Schenk, J.; Naseri Seftejani, M.; Spreitzer, D.; Zarl, M. The Way to A Carbon Free Steelmaking. In Proceedings of the 3rd ADMET 2018, Lviv, Ukraine, 10–13 June 2018.
22. Bäck, E.; Badr, K.; Plaul; J.F.; Sormann, A. Überblick über die Entwicklung der Wasserstoff-Schmelzreduktion am Lehrstuhl für Metallurgie. *BHM Berg-und Hüttenmännische Mon.* **2009**, *154*, 6–9.
23. Naseri Seftejani, M.; Schenk, J.; Spreitzer, D.; Andreas Zarl, M. Slag Formation during Reduction of Iron Oxide Using Hydrogen Plasma Smelting Reduction. *Materials* **2020**, *13*, 935.